Journal of Power Sources 189 (2009) 256–262

Contents lists available at ScienceDirect

Journal of Power Sources

journal homepage: www.elsevier.com/locate/jpowsour

The effect of carbon coating thickness on the capacity of $LiFePO_4$/C composite cathodes

Yung-Da Cho [a], George Ting-Kuo Fey [a,*], Hsien-Ming Kao [b]

[a] Department of Chemical and Materials Engineering, National Central University, Chung-Li 32054, Taiwan
[b] Department of Chemistry, National Central University, Chung-Li 32054, Taiwan

ARTICLE INFO

Article history:
Received 14 July 2008
Received in revised form
10 September 2008
Accepted 15 September 2008
Available online 25 September 2008

Keywords:
$LiFePO_4$
Carbon coating
Coating thickness
Vapor deposition technique
Cathode
Li-ion batteries

ABSTRACT

Two types of carbon source and precursor mixing pellets were employed simultaneously to prepare the $LiFePO_4$/C composite materials: Type I using the $LiFePO_4$ precursor with 20 wt.% polystyrene (PS) as a primary carbon source, and Type II using the $LiFePO_4$ precursor with 50 wt.% malonic acid as a secondary carbon vapor source. During final sintering, a Type I pellet was placed down-stream and Type II precursor pellet(s) was(were) placed upstream next to a Type I precursor pellet in a quartz-tube furnace. The carbon-coated product of the sintered Type I precursor pellet was obtained by using both PS and malonic acid as carbon sources. When two Type II pellets were used as a carbon vapor source (defined as Product-2), a more uniform film between 4 and 8 nm was formed, as shown in the TEM images. In the absence of a secondary carbon source (defined as Product-0), the discharge capacity of Product-0 was 137 mAh g^{-1} with 100 cycles at a 0.2*C*-rate, but Product-2 demonstrated a high capacity of 151 mAh g^{-1} with 400 cycles. Our results indicate that electrochemical properties of $LiFePO_4$ are correlated to the amount of carbon and its coating thickness and uniformity.

1. Introduction

The olivine structure of $LiFePO_4$ was first reported by Dr. Goodenough's group in 1997 [1,2] as a potential cathode material for lithium-ion batteries. It has the advantages of high energy density [3,4], high theoretic capacity of 170 mAh g^{-1} [5–7], high charge/discharge potential (3.4 V versus Li^+/Li) [3,8], low costs [9–12] and environmental friendliness [13–15], and shows good cycle stability during the charge/discharge process [16–18]. In particular, it has a stable three dimensional framework due to strong P–O covalent bonds in $(PO_4)^{3-}$ polyanion preventing the P–O bonds from breaking and releasing oxygen at high states of charge [19]. This characteristic provides excellent safety and stable operation of battery even under unusual conditions [20], and high temperatures [21].

The main disadvantages of $LiFePO_4$ materials are poor electronic conductivity [22–25], slow lithium-ion diffusion [26–29], low tap density [4] and poor batch reproducibility [15]. In order to enhance the electronic conductivity and electrochemical properties of $LiFePO_4$ cathode materials, many researchers have suggested that carbon coating [4–5,15–17] and metal doping can be used [23,30–34], as well as the synthesis of nanoparticles [1–3,10,35]. In an earlier study, Ravet et al. [36] reported that $LiFePO_4$ had a capacity of about 160 mAh g^{-1} when coated with about 1 wt.% carbon and cycled at a 1*C*-rate at 80 °C. They added sucrose as a carbon source, during synthesis thereby obtaining carbon-coated particles directly, which indicates that increasing the conductivity can improve the capacity significantly. Huang et al. [5] manufactured an $LiFePO_4$/C composite by mixing raw materials with a carbon gel before heating. In this composite, $LiFePO_4$ has a particle size of 100–200 nm and contains about 15 wt.% carbon, and first demonstrated that $LiFePO_4$ could have excellent rate capability. Even when cycled at a 5*C*-rate, it demonstrated a capacity of about 120 mAh g^{-1}. Huang et al. believe that both particle size minimization and intimate carbon contact are needed to optimize the rate capability of this material. However, these approaches suffer from the problems of complex manufacturing processes and firing at high temperatures for long periods in order to obtain a single-phase, olivine-type $LiFePO_4$. Chen and Dahn [4] prepared $LiFePO_4$ samples containing 3.5 wt.% coated-carbon with a discharge of 160 mAh g^{-1}, very close to the theoretical capacity. The positive effects of coated-carbon for electrode materials were also suggested by Cushing and Goodenough, who believed that it could not only improve the electronic conductivity between particles, but also provide electronic tunnel to complement the charge equilibrium

* Corresponding author. Tel.: +886 3 425 7325/422 7151x34206; fax: +886 3 425 7325.
E-mail address: gfey@cc.ncu.edu.tw (G.T.-K. Fey).

0378-7753/$ – see front matter © 2008 Elsevier B.V. All rights reserved.
doi:10.1016/j.jpowsour.2008.09.053

during Li extraction/insertion [37]. In the above literature, many researchers attempted coating $LiFePO_4$ particles with only one carbon source by incorporating an organic or polymeric component with the precursors before firing.

In previous work, we have developed various methods that involve carbon coating [38–40] and metal doping [40]. In our carbon coating process, we found that carbon coating thickness and structure play important roles in determining the capacity of $LiFePO_4$ cathode materials. Therefore, in this paper, we investigated the effect of carbon coating thickness and its homogeneity (uniformity) on the electrochemical properties of $LiFePO_4$/C composite materials prepared by a carbon vapor deposition technique, and used both polystyrene and malonic acid as carbon sources. The physical, structural, and Li-ion diffusion kinetics of $LiFePO_4$/C composites were systematically investigated.

2. Experimental

The $LiFePO_4$ precursor powders were prepared by the solid state reaction method using Li_2CO_3 (99%, Aldrich), $FeC_2O_4{\cdot}2H_2O$ (98.5%, Aldrich), and $NH_4H_2PO_4$ (98.5%, Showa) as the starting materials, which were weighed in stoichiometric amounts, then mixed and ground in a planetary ball-mill with a rotation speed of 250 rpm for 3 h in acetone under an argon atmosphere. The mixture was preheated at 593 K at a 5 K min^{-1} heating rate and held at 593 K for 10 h under Ar/H_2 (v/v 95:5) atmosphere, in order to obtain gray $LiFePO_4$ precursor powders. Before final sintering, two types of carbon source and precursor mixing pellets were prepared: Type I using 20 wt.% polystyrene (PS) as a primary carbon source, and Type II using 50 wt.% malonic acid (98%, Aldrich) as a secondary carbon source. Both carbon source and precursor mixing pellets were prepared by ball-milling a mixture of $LiFePO_4$ precursor and carbon sources for 1 h, and pressing it into pellets. During final sintering, a Type I precursor pellet was placed down-stream and Type II precursor pellet(s) was(were) placed upstream next to a Type I precursor pellet in a quartz-tube furnace at 873 K under flowing Ar/H_2 (v/v 95:5) for 12 h. Fig. 1 is a schematic diagram of carbon vapor deposition method. A reducing atmosphere was employed during the calcination process in order to avoid the oxidation of Fe^{2+} cations. Consequently, the carbon-coated surface of the sintered Type I precursor pellet was from dual carbon sources: PS and malonic acid. Product-1, Product-2, or Product-3 is defined as the above sintering product made from arranging a Type I precursor pellet next to one, two, or three piece(s) of Type II precursor pellet(s), respectively. Product-0 was the product that used only a primary carbon source. Pure $LiFePO_4$ was prepared directly from the starting materials of precursor without using any additional carbon coating source and it may contain trace amounts of carbon derived from the starting materials of precursor.

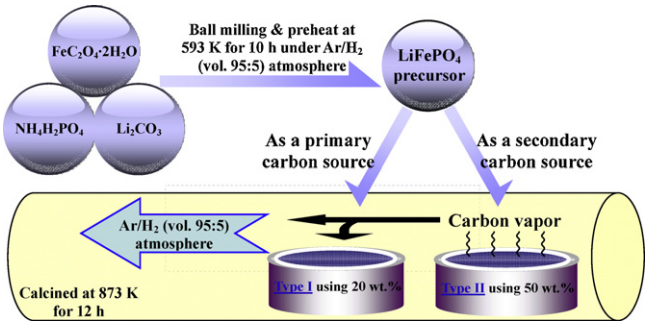

Fig. 1. A schematic diagram of carbon vapor deposition.

An X-ray diffractometer (XRD), Siemens D-5000, Mac Science MXP18, equipped with a nickel-filtered Cu-K_α radiation source (λ = 1.5405 Å) was used for structural analysis. The microstructure and lattice images of the coated particles were observed with a high resolution transmission electron microscope (HRTEM, Hitachi HF 2000) equipped with a LaB_6 gun. Electron diffraction patterns were obtained through selected area electron diffraction (SAED). The chemical composition of the separated phases was determined by nanobeam energy dispersive spectroscopy (EDS). For these experiments, samples were previously dispersed in acetone and deposited on a holey silicon grid.

Carbon content analyses of the products were investigated on a OIA Model Solids module as the total organic carbon (TOC) analyzer apparatus. Raman spectroscopy was performed on samples of powders using a ISA T64000 double beam pass spectrometer equipped with a microscope stage for analyzing small samples utilizing 180° incident geometry. A Spectra Physics argon-ion laser was employed to excite laser Raman spectra using a 515 nm laser line at an incident power of ca. 10 mW. The electronic conductivity of samples was measured by four-point conductivity measurements of Keithley Model 2400S source meter. In DSC analysis, after the cell charged to 4.5 V and was disassembled in the glovebox, the sample was removed from the aluminum current collector and transferred to the sample holder. The samples were analyzed by the DSC unit using a temperature scan rate of 10 K min^{-1}.

Experimental test cells for measurements used the cathode with a composition of 85 wt.% active material, 10 wt.% conductive carbon black, and 5 wt.% poly(vinylidene fluoride) in N-methyl-2-pyrrolidone (NMP), as the solvent for the mixture, which was then applied onto an etched aluminum foil current collector and dried at 393 K for 3 h in an oven. The separator used was a Celgard 3501 microporous polypropylene membrane. The electrolyte was 1 M $LiPF_6$ in ethylene carbonate: diethyl carbonate EC:DEC (1:1, v/v) (Tomiyama Chemicals). A lithium metal (Foote Mineral) anode was used in this study. The cells were assembled in a glove box filled with argon gas. The charge/discharge cycling was galvanostatically performed at a current of 0.2 C with cut-off voltages of 2.8 and 4.0 V (versus Li/Li^+) at 298 K in a multi-channel battery tester (Maccor 4000).

Phase transitions occurring during the cycling processes were examined by slow scan cyclic voltammetry, performed with a Li-ion coin cell. The electrolyte used was the same as that for the coin cell. Cyclic voltammograms were run on a Solartron 1287 Electrochemical Interface at a scan rate of 0.1 mV s^{-1} between 3.0 and 4.0 V.

3. Results and discussion

3.1. XRD analysis

The XRD patterns of pure $LiFePO_4$, Product-0 and Product-2 are shown in Fig. 2. All diffraction lines were indexed to an orthorhombic crystal structure (space group P_{mnb}, triphylite). However, some impurity Li_3PO_4 peaks (marked with stars) are observed in pure $LiFePO_4$ as shown in Fig. 2a. From Fig. 2b and c, no phase impurities such as Fe_2P phosphide were detected on the $LiFePO_4$/C samples, which mean that the olivine structure was maintained after our carbon coating process. Additionally, the profiles of the reflection peaks are quite narrow and symmetric. Thereby, a well-crystallized product is obtained. The grain size (D) was calculated with the Scherrer formula: $\beta\cos(\theta) = k\lambda/D$, where β is the full-width-at-half-maximum length of the (0 2 0) reflection [41] and k is a constant here close to unity. The mean value of D of pure $LiFePO_4$, Product-0 and Product-2 were 310 Å, 210 Å and 204 Å, respec-

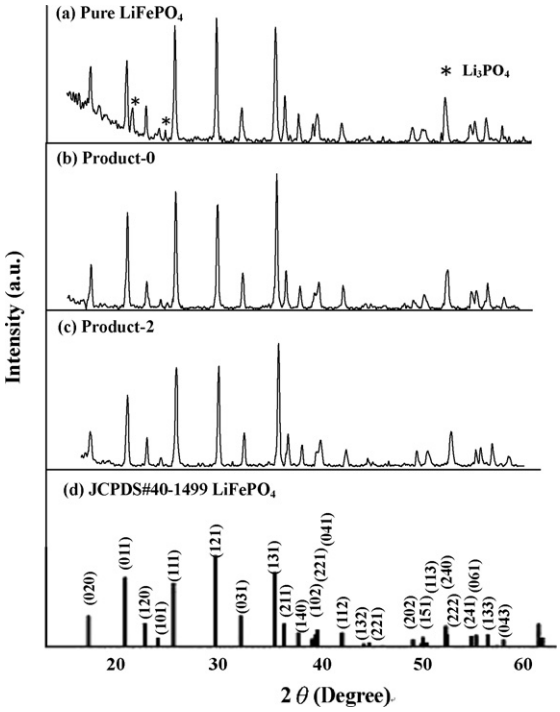

Fig. 2. X-ray diffraction patterns of (a) pure $LiFePO_4$; (b) Product-0; (c) Product-2; (d) JCPDS #40-1499 $LiFePO_4$.

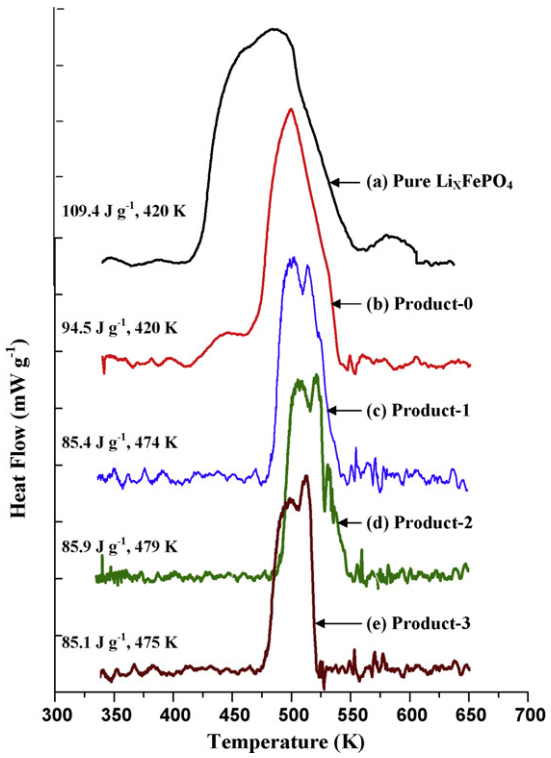

Fig. 3. DSC profiles of (a) pure $LiFePO_4$; (b) Product-0; (c) Product-1; (d) Product-2; (e) Product-3. Charged to 4.5 V.

tively. It is known that adding carbon restrains particle growth [42].

3.2. DSC analysis

Since safety and thermal stability have become a necessity for Li-ion batteries, we studied the thermal stability of 4.5 V charged cathodes by DSC analysis. Fig. 3 shows the DSC results for different $LiFePO_4$ composite electrodes in the temperature range 330–650 K at a heating rate of 10 K min^{-1}. For the pure $LiFePO_4$ sample, the exothermic heat flow was detected under a wide temperature range of 420 to 575 K, with total heat evolution ~109.41 J g^{-1}. The exothermic heat flow strongly depends on the synthesis method and test conditions, and various exothermic peaks at about 543 and 633 K with different values for the total heat flow have been reported by various researchers [13,41]. The total heat flow value was about 312 J g^{-1}.

For Product-0 sample, the exothermic heat flow was detected in the range of ~420 to 550 K, with total heat flow value of about 94.5 J g^{-1}. The samples with secondary carbon vapor have a lesser exothermic heat flow range of ~475 to 550 K. However, the total heat evolution was very similar. For the optimized composition of Product-2, the total heat evolution was about 85.9 J g^{-1}. From these thermal data, it is clear that exothermic heat flow can be reduced further by carbon vapor deposition. Moreover, the onset temperature can be raised from 420 to 475 K.

When compared to the results of other cathode materials reported in the literature, $LiFePO_4$ is superior [44], This exceptional thermal stability is attributed to the unique anion bonding and stability of phosphate materials with their shorter P–O bond and more tightly bound oxygen.

3.3. TEM/SAED/EDS analysis

In order to understand the carbon coating thickness and structure on the surface of $LiFePO_4$ particles, we conducted HRTEM analysis of $LiFePO_4$/C particles in combination with SAED and EDS. Fig. 4 shows the TEM images of $LiFePO_4$/C composite materials derived from Product-1, Product-2, and Product-3. Carbon coating thickness increased with the number of pellets of the Type II precursor. When using one Type II pellet as a secondary carbon vapor source, Product-1 contributed to a thin film about 2 nm thick (Fig. 4a) over most of the surface area and a thicker layer measuring about 15 nm (Fig. 4c) in certain areas. However, when using two Type II pellets, Product-2 displayed a more uniform film between 4–8 nm (Fig. 4d–f) around the particles. Further, when using three Type II pellets, Product-3 gave a much thicker coating layer about 10–25 nm (Fig. 4g–i).

From SAED analysis, Figs. 4k, m and o show a hollow ring pattern and some bright spots in the outer carbon coating layer, which suggest that some amount of graphite-like carbon was in the very disordered carbon structure for the three samples. The dark area exhibits a bright spot pattern in the core that is typical for crystalline $LiFePO_4$ as displayed in Figs. 4j, l and n. Thus, amorphous and graphite-like carbon films were clearly identified on the outer surface of the particles. Those results were consistent with Fey's results [38]. Fey et al. pointed out that the TEM micrograph of $LiFePO_4$/C consists of two parts: a dark region and a grayish region that surrounds the dark region, and from SAED patterns indicate that the materials of interest were in a crystalline phase. The TEM/EDS results unambiguously show that the particles in the dark region are $LiFePO_4$ with a trace of carbon and those in the grayish region are carbon only. In addition, our EDS analysis confirmed that the dark area includes Fe, P, O, and C components (Fig. 4p–r).

3.4. Carbon analysis

The actual carbon content in the $LiFePO_4$/C composites was measured by total organic carbon (TOC) analysis. Samples were pressed into disk-shaped pellets and their electronic conductiv-

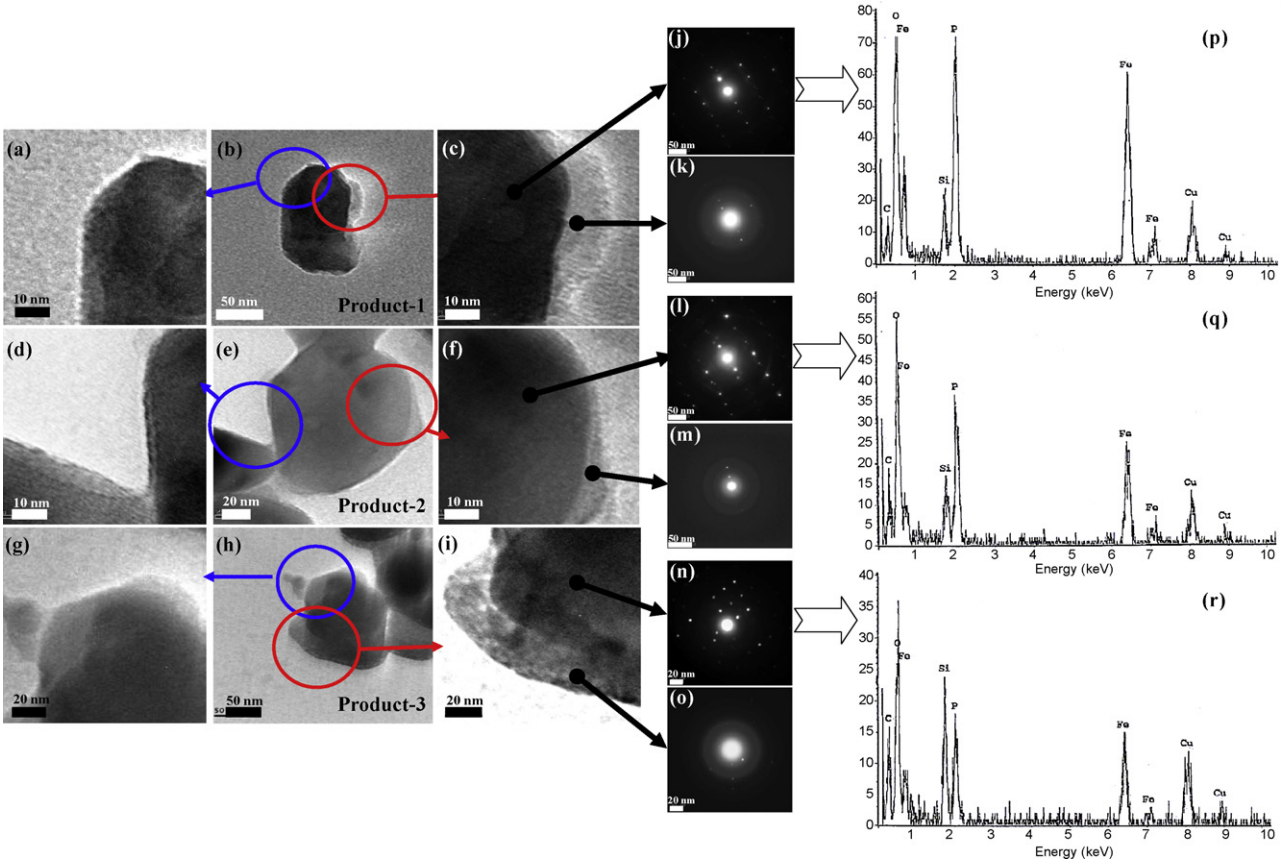

Fig. 4. (a)–(i) TEM micrographs of various $LiFePO_4$/C powders; (j)–(o) SAED for the $LiFePO_4$/C particles; (p)–(r) EDS analysis for the $LiFePO_4$/C particles.

ities measured by the four-point dc method. Table 1 presents a comparison of conductivity, carbon content, carbon coating thickness, and discharge capacity for the bare $LiFePO_4$, Product-0, Product-1, Product-2, and Product-3. It is clear that carbon content also increased with the pellet number of Type II precursor. All the $LiFePO_4$/C samples exhibited high electronic conductivity of 10^{-4} S cm^{-1} at 300 K. As shown in Table 1, the conductivity increased along with the carbon content of samples, and the carbon content was between 1.25 and 2.54 wt.%. The individual $LiFePO_4$ particle was coated with carbon layer, and carbon layer provides a conductive network. Therefore, it could dramatically increase conductivity of the material.

Raman spectroscopy is a particularly useful tool for characterizing the structure of the carbon coating layer on the particles surface. Fig. 5 and Table 2 display the Raman spectra of the composites in the range of 800–1700 cm^{-1}. In all samples, the spectra had a relatively small band at 950 cm^{-1} corresponding to the symmetric PO_4^{3-} stretching vibration in olivine structure [45]. Two intense broad bands located at ~1360 and ~1600 cm^{-1} dominated every spectrum of the $LiFePO_4$ samples. Doeff et al. [19,46] pointed out that the two broad bands can actually be deconvoluted into four peaks at around 1190, 1350, 1518, and 1590 cm^{-1}. The ones at around 1190 and 1518 cm^{-1} can be assigned to sp^3-type carbon, while the others are the D (disordered) band (1350 cm^{-1}) and G (graphene) band (1590 cm^{-1}) of sp^2-type carbon. The I_D/I_G ratio roughly correlates to the amount of the graphene clusters in the disordered carbon, with smaller ratios being associated with higher electronic conductivity. Through deconvolution, it is also possible to determine sp^3/sp^2 ratios with smaller ratios correlating to a more graphitic nature and higher conductivity, and further enhance the electrochemical performance of $LiFePO_4$ material.

It can be seen in Table 2, the I_D/I_G ratios decreased as the Type II carbon vapor pellet increased, and the electronic conductivity also increased (as shown in Table 1). It is interesting to note that the samples made with the secondary carbon sources (malonic acid) have lower I_D/I_G ratios, suggesting that the malonic acid modifies the structure of the carbon as well as increases the amount of graphene clusters. These results were consistent with Doeff's suppositions [38]. This effect can be explained that some amounts of graphite-like carbon in the disordered carbon structure, and consequently enhanced electronic conductivity of the carbon deposit. Improved electronic properties of the residual carbon can provide

Table 1
A Comparison of the conductivity, carbon content, carbon thickness, and discharge capacity of samples.

Materials	Electronic conductivity (S cm^{-1})	Carbon content (wt.%)	Carbon thickness (nm)	Discharge capacity (mAh g^{-1})	Synthesis condition
Pure $LiFePO_4$	5.88×10^{-8}	0.02	0	7th = 99	
Product-0	6.42×10^{-4}	1.25	2–6	7th = 137	
Product-1	6.99×10^{-4}	1.67	2–15	7th = 141	873 K, 12 h
Product-2	7.11×10^{-4}	2.28	4–8	7th = 151	
Product-3	8.76×10^{-4}	2.54	10–25	7th = 143	

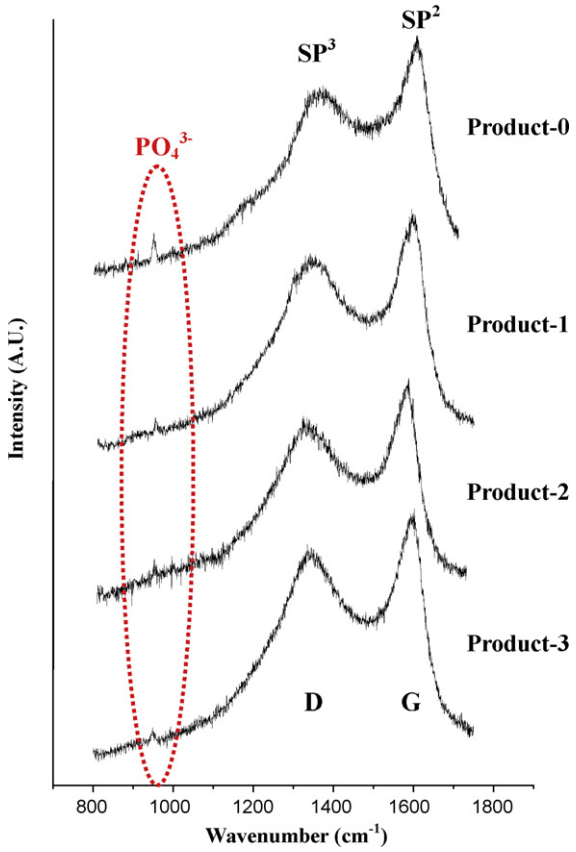

Fig. 5. Raman spectra of various $LiFePO_4$ samples.

better electrode's performance, this is confirmed by the later cell performance.

3.5. Electrochemical properties

The capacity and cyclability of the $LiFePO_4$ electrode was determined between 4.0 and 2.8 V by galvanostatic charge/discharge testing at a 0.2*C*-rate. Fig. 6 compares the discharge capacity of pure $LiFePO_4$ with various $LiFePO_4$/C samples, while Fig. 7 shows the charge/discharge voltage profiles in the first cycle for various $LiFePO_4$ electrodes. The voltage difference between the flat charge and discharge plateaus (ΔV) in Fig. 7 is related to the polarization of the cell system. The smaller the ΔV, the less the polarization.

For the pure $LiFePO_4$ sample, the first discharge capacity was only 104 mAh g^{-1} due to low electronic conductivity (see Table 1, 5.88×10^{-8} S cm^{-1}) and large ΔV of 0.32 V. When there was only one primary carbon source, Product-0 displayed a maximum discharge capacity of 137 mAh g^{-1}. When one type II pellet was used as

Table 2
Raman spectra peak intensity and I_D/I_G ratio of samples.

Items	Raman			Condition
	Peak (cm^{-1})	Intensity (A.U.)	I_D/I_G ratio	
Product-0	SP^3 1366 SP^2 1609	1891 1988	0.9512	873 K, 10 h
Product-1	SP^3 1365 SP^2 1606	1521 1601	0.9500	
Product-2	SP^3 1360 SP^2 1612	1448 1531	0.9458	
Product-3	SP^3 1361 SP^2 1601	1361 1448	0.9399	

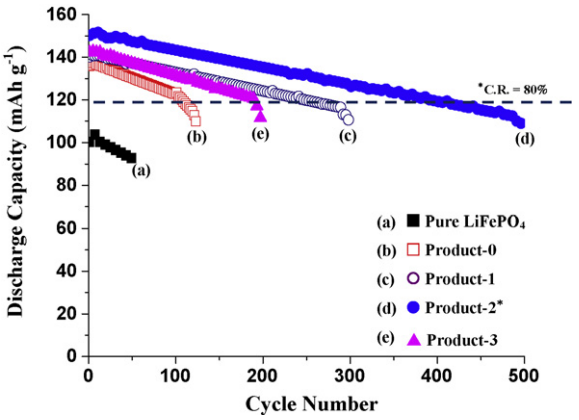

Fig. 6. Discharge capacity versus cycle number for various $LiFePO_4$ electrodes. Charge/discharge: 4.0/2.8 V; 0.2 C-rate.

a carbon vapor source, Product-1 demonstrated a maximum capacity of 141 mAh g^{-1}. With two Type II pellets, Product-2 displayed the best electrochemical performance with a first discharge capacity of 148 mAh g^{-1} and the smallest ΔV of 0.19 V in Fig. 7. The discharge capacity of Product-2 gradually increased with cycling and reached the highest level at 151 mAh g^{-1} after 7 cycles, due to the suitable carbon content which formed a thin and uniform carbon conductive film over the whole particle surface (as shown from TEM images in Figs. 4 d and f), which improved the conductivity (7.11×10^{-4} S cm^{-1}) and contact between the electrolyte and the active phase. As a result, Product-2 provided the best cycle life of about 400 cycles in this study.

However, using three Type II pellets caused the discharge capacity to drop to 143 mAh g^{-1} for the Product-3 electrode because of high carbon content (2.54 wt.%), thicker carbon coating layer (~10–25 nm) and large ΔV of about 0.36 V. Furthermore, when the carbon content was increased, the inactive carbon reduced the ratio of the active material, leading to a decrease in capacity. In addition, the carbon coating network is an intrinsically inert material for Li^+ storage, hindering Li^+ diffusion and resulting in a decrease in discharge capacity. Above all, the large ΔV value of 0.36 V exemplified the short cycle life of less than 200 cycles for the Product-3 electrode. Therefore, the above results are evident that electrochemical properties of $LiFePO_4$ are correlated to the amount of carbon and its coating thickness and uniformity.

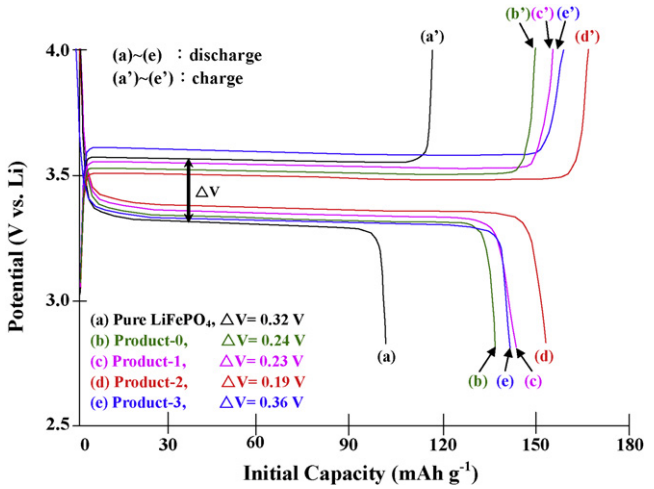

Fig. 7. Initial charge and discharge curves for various $LiFePO_4$ electrodes. (a)–(e): discharge; (a′)–(e′): charge.

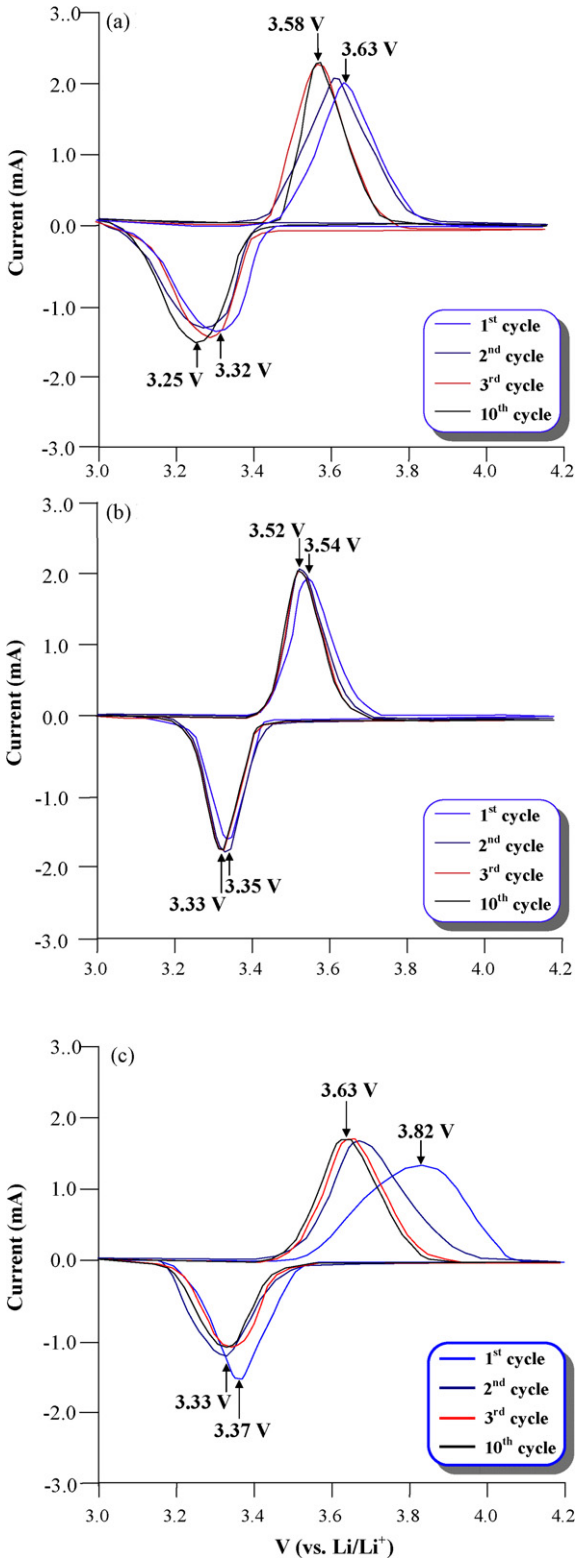

Fig. 8. Cyclic voltammograms of $LiFePO_4$ electrodes between 3.0 and 4.2 V at the scanning rate of 0.1 mV s^{-1}.

As shown in Fig. 7, the voltage difference between the flat charge and discharge plateaus (ΔV) is related to the polarization of the cell system, and the voltage difference ($\Delta V'$) between the anodic and cathodic peaks of the same cycle is correlated to the polarization or reversibility of the redox reaction: the smaller the $\Delta V'$, the lower the polarization or the greater the reversibility. In turn, this leads to greater cycle stability. Since passivation occurs when the redox reaction proceeds, it usually increases or is barely changed with the reaction. For simplicity, we always compare the initial $\Delta V'$ value as a standard to estimate the passivation or polarization levels. Fig. 8 shows the cyclic voltammograms of the $LiFePO_4$/C composite electrodes measured between 3.0 and 4.2 V to characterize the redox reactions, in which the voltage difference ($\Delta V'$) between the anodic and cathodic peaks can be easily measured. Fig. 8b clearly demonstrates that the Product-2 electrode exhibited the smallest $\Delta V'$ of 0.21 V among the three samples at beginning, indicating low polarization and high reversibility, as evidenced by a long cycle life of 400 cycles shown in Fig. 6. On the contrary, Fig. 8a and c display large $\Delta V'$s about 0.32 and 0.45 V for the Product-1 and Product-3 electrodes, respectively. This indicates that extra amounts of carbon coating adversely affected the polarization and cycle life of the cell, resulting in a cycle life of about 300 cycles and 200 cycles for Product-1 and Product-3, respectively.

It can be seen from Fig. 8b that Product-2 exhibits much sharper current peaks with little change in current intensity and delivers higher capacity (154 mAh g^{-1}) with lower voltage polarization about 0.21 V than Product-1 and Product-3, indicating that the composite has an improved electrochemical kinetics and proper passivation layer due to more uniform carbon coating film. In practice, the current intensity in cyclic voltammograms is related to the passivation level of the electrode surface: the higher the current intensity, the lower the passivation level or the higher the reactivity. For Product-2, little change in current intensity observed after 10 cycles reveals that the uniform carbon coating film of 4–8 nm in this study provided a proper passivation layer for the redox reaction.

The CV peak currents, I_p, during anodic scans were used to evaluate the Li^+ diffusion coefficient D, applying the Randles Sevcik equation:

$$I_p = 2.69 \times 10^5 n^{3/2} A D^{1/2} v^{1/2} C$$

where A is the electrode area (cm^2), n is the number of electrons involved in the redox process (1 in our case), C is the shuttle concentration (mol cm^{-3}), v is the potential scan rate (V s^{-1}), I_p is in units of amperes, and D is in units of cm^2 s^{-1}. Using the above equation, the Li^+ diffusion coefficients of Product-1, Product-2 and Product-3 were calculated as 9.20×10^{-12}, 4.56×10^{-12} and 5.91×10^{-13} cm^2 s^{-1}, respectively. Thus, the $LiFePO_4$/C composite with a higher carbon coating layer exhibited slower lithium ion diffusion due to the thick carbon layer resulting in an increase of polarization.

4. Conclusion

Using a carbon vapor deposition technique, we have shown that the amount of carbon and its coating thickness and uniformity in $LiFePO_4$/C materials are all crucial parameter in determining the electrochemical performance. $LiFePO_4$ coated with a thin and uniform carbon film can deliver maximum discharge capacity of 151 mAh g^{-1} at a 0.2C-rate and sustain 415 cycles at 80% of capacity retention. In order to minimize the polarization, a carbon coating layer must be uniformly distributed around each active particle, because the lower polarization leads to a higher reversible capacity.

Acknowledgements

The authors thank Prof. W. H. Li (Department of Physics, National Central University) for his valuable suggestions and the use of Raman spectrometer. Financial support for this work was provided

by the National Science Council of the Republic of China under contract No. NSC 97-2221-E-008 -052.

References

[1] A.K. Padhi, K.S. Nanjundoswamy, J.B. Goodenough, J. Electrochem. Soc. 144 (1997) 1188.
[2] A.K. Padhi, K.S. Nanjundaswamy, C. Masquelier, S. Okada, J.B. Goodenough, J. Electrochem. Soc. 144 (1997) 1609.
[3] S. Franger, F. Le Cras, C. Bourbon, H. Rouault, Electrochem. Solid-State Lett. 5 (2002) 231.
[4] Z. Chen, J.R. Dahn, J. Electrochem. Soc. 149 (2002) A1184.
[5] H. Huang, S.C. Yin, L.F. Nazar, Electrochem. Solid-State Lett. 4 (2001) A170.
[6] P.P. Prosini, M. Carewska, S. Scaccia, P. Wisniewski, S. Passerini, M. Pasquali, J. Electrochem. Soc. 149 (2002) A886.
[7] J. Barker, M.Y. Saidi, J.L. Swoyer, Electrochem. Solid-State Lett. 6 (2003) A53.
[8] S. Okada, S. Sawa, M. Egashira, J.I. Yamaki, M. Tabuchi, H. Kageyama, T. Konishi, A. Yoshino, J. Power Sources 97–98 (2001) 430.
[9] A.S. Anderesson, J.O. Thomas, J. Power Sources 97–98 (2001) 498.
[10] F. Croce, A.D. Epifanio, J. Hassoun, A. Deptula, T. Olczac, B. Scrosati, Electrochem. Solid State Lett. 5 (2002) A47.
[11] G. Arnold, J. Garche, R. Hemmer, S. Ströbele, C. Volger, M. Wohlfart-Mehrens, J. Power Sources 119–121 (2003) 247.
[12] K.S. Park, J.T. Son, H.T. Chung, S.J. Kim, C.H. Lee, K.T. Kang, H.G. Kim, Solid State Commun. 129 (2004) 311.
[13] A. Yamada, S.C. Chung, K. Hinokuma, J. Electrochem. Soc. 148 (2001) A224.
[14] X.Z. Liao, Z.F. Ma, L. Wang, X.M. Zhang, Y. Jiang, Y.S. He, Electrochem. Solid-State Lett. 7 (2004) A522.
[15] C.H. Mi, X.B. Zhao, G.S. Cao, J.P. Tu, J. Electrochem. Soc. 152 (2005) A483.
[16] J. Shim, K.A. Striebel, J. Power Sources 119–121 (2003) 955.
[17] S.T. Myung, S. Komaba, N. Hirosaki, H. Yashiro, N. Kumagai, Electrochim. Acta 49 (2004) 4213.
[18] K. Amine, J. Liu, I. Belharouak, Electrochem. Commun. 7 (2005) 669.
[19] Y. Hu, M.M. Doeff, R. Kostecki, R. Finones, J. Electrochem. Soc. 151 (2004) A1279.
[20] D. Wang, X. Wu, Z. Wang, L. Chen, J. Power Sources 140 (2005) 125.
[21] M. Takahashi, S. Tobishima, K. Takei, Y. Sakurai, Solid State Ion. 148 (2002) 283.
[22] A.S. Andersson, B. Kalska, L. Haggstrom, J.O. Thomas, Solid State Ion. 130 (2000) 41.
[23] S.Y. Chung, J.T. Bloking, Y.M. Chiang, Nat. Mater. 1 (2002) 123.
[24] P.S. Herle, B. Ellis, N. Coombs, L. Nazar, Nat. Mater. 3 (2004) 147.
[25] A. Yamada, M. Hosoya, S.C. Chung, Y. Kudo, K. Hinokuma, K.Y. Liu, Y. Nishi, J. Power Sources 191–121 (2003) 232.
[26] N. Ravet, Y. Chouinard, J.F. Magnan, S. Besner, M. Gauthier, M. Armand, J. Power Sources 97–98 (2001) 503.
[27] S.F. Yang, Y.N. Song, P.Y. Zavalij, M.S. Whittingham, Electrochem. Commun. 4 (2002) 239.
[28] H.T. Chung, S.K. Jang, H.W. Ryu, K.B. Shim, Solid State Commun. 131 (2004) 549.
[29] R. Amin, P. Balaya, J. Maier, Electrochem. Solid-State Lett. 10 (2007) A13.
[30] J.F. Ni, H.H. Zhou, J.T. Chen, X.X. Zhang, Mater. Lett. 59 (2005) 236.
[31] P.S. Herle, B. Ellis, N. Coombs, L.F. Nazar, Nat. Mater. 3 (2004) 147.
[32] J.F. Ni, H.H. Zhou, J.T. Chen, X.X. Zhang, Mater. Lett. 59 (2005) 2361.
[33] M. Abbate, S.M. Lala, L.A. Montoro, J.M. Rosolen, Electrochem. Solid-State Lett. 8 (2005) A288.
[34] G.X. Wang, S. Bewlay, J. Yao, J.H. Ahn, S.X. Dou, H.K. Liu, Electrochem. Solid-State Lett. 7 (2004) A503.
[35] H. Huang, S.C. Yin, T. Kerr, N. Taylor, L.F. Nazar, Adv. Mater. 3 (2004) 147.
[36] N. Ravet, J.B. Goodenough, S. Besner, M. Simoneau, P. Hovington, M. Armand, Proceedings of the 196th ECS Meeting, Hawaii, 17–22 October 1999.
[37] B.L. Cushing, J.B. Goodenough, Solid State Sci. 4 (2002) 1487.
[38] G.T.K. Fey, T.L. Lu, J. Power Sources 178 (2008) 807.
[39] G.T.K. Fey, T.L. Lu, J. Solid State Electrochem. 12 (2008) 825.
[40] Y.D. Cho, G.T.K. Fey, J. Solid State Electrochem. 12 (2008) 815.
[41] B.D. Cullity, S.R. Stock, Elements of X-ray Diffraction, 3rd ed., Prentice Hall Publishers, NJ, USA, 2001 (Chapter 5.2).
[42] T. Takeuchi, M. Tabuchi, A. Nakashima, T. Nakamura, Y. Miwa, H. Kageyama, K. Tatsumi, J. Power Sources 146 (2005) 575.
[44] Z. Zhang, D. Fouchard, J.R. Rea, J. Power Sources 70 (1998) 16.
[45] C.M. Burba, R. Frech, J. Electrochem. Soc. 151 (2004) A1032.
[46] M.M. Doeff, Y. Hu, F. McLarnon, R. Kostecki, Electrochem. Solid-State Lett. 6 (2003) A207.